ASSESSMENT OF THERMAL CONDITIONS IN URBAN AREAS WITH USE OF DIFFERENT SATELLITE DATA AND GIS

Jakub Walawender[1,2] and Monika Hajto[3]

[1] Satellite Remote Sensing Centre, Institute of Meteorology and Water Management, Krakow, Poland;
[2] Department of Climatology, Institute of Geography and Spatial Management, Jagiellonian University, Krakow, Poland;
[3] Department of Air Pollution Monitoring and Modelling, Institute of Meteorology and Water Management, Krakow, Poland;
e-mail: jakub.walawender@imgw.pl, monika.hajto@gmail.com

Abstract

This methodological case study examines different satellite data (Terra/MODIS, Meteosat/SEVIRI, NOAA/AVHRR and Landsat/TM) and different land surface temperature retrieval algorithms in terms of urban heat islands monitoring. Four land surface temperature maps were created in order to perform comparative analysis of the selected sensors and mathematical formulas for the land surface temperature estimation. Most of the data processing was done within GIS environment. The study area is city of Krakow (Poland). All of the satellite images used in the study were obtained on July 22, 2007 at about 9:00-9:30. Some advantages and disadvantages of selected sensors are depicted. Revision of reference papers and web pages is included.

INTRODUCTION

Satellite data are still more and more widely used for various environmental applications. One of the most commonly applied procedures performed with the use of remotely sensed data is land surface temperature (LST) retrieval, which is very important among others for urban heat islands monitoring. There are many different satellite date available with different spatial, spectral and temporal resolution as well as there are many algorithms for LST retrieval. The main objective of this study is to review and evaluate selected algorithms for land surface temperature retrieval with use of satellite data obtained by four different operational satellite sensors: Meteosat/SEVIRI, NOAA/AVHRR, Terra/MODIS and Landsat/TM. Three images obtained on July 22, 2007 at about 9:30 UTC and MODIS image obtained at 9:00 UTC are used for this comparative analysis.

Before extracting land surface temperatures from thermal bands, the images were geometrically and radiometrically corrected. Next step was to convert spectral radiance to radiant (black body) temperature. This procedure requires implementing Planck's law, which describes emissivity of a black body depending on wavelength and absolute temperature. Then the radiant temperature was recalculated to land surface (kinetic) temperature including atmosphere influence and emissivity correction. Most of the data processing steps were done within GIS environment.

Acquired four surface temperature maps were compared with each other in order to define possible application of the satellite data with different spatial and temporal resolution. Some advantages and disadvantages of each sensor with respect to land surface temperature retrieval are indicated and discussed. Wide list of revised reference papers and web pages is included.

STUDY AREA

The city of Krakow is located in southern Poland (Fig. 1). Together with neighbouring towns, Krakow form an urban-industrial agglomeration (Fig. 2) with recognized heat island having two maxima, one connected with the city centre (**1**) and the other with steelworks (**2**) located in the eastern part. The city urban structure is diversified: continuous built up area predominates in the city centre which is surrounded by living and industrial districts. These are further encircled by blocks of flats. The further from the centre, buildings are more detached and contribution of green areas rises. Small heat islands were also identified in the satellite towns located in the neighbourhood of Krakow, e.g.: Skawina (**3**), Wieliczka (**4**), Wadowice (**5**), Myślenice (**6**), Bochnia (**7**), Krzeszowice (**8**), Olkusz (**9**), Miechów (**10**).

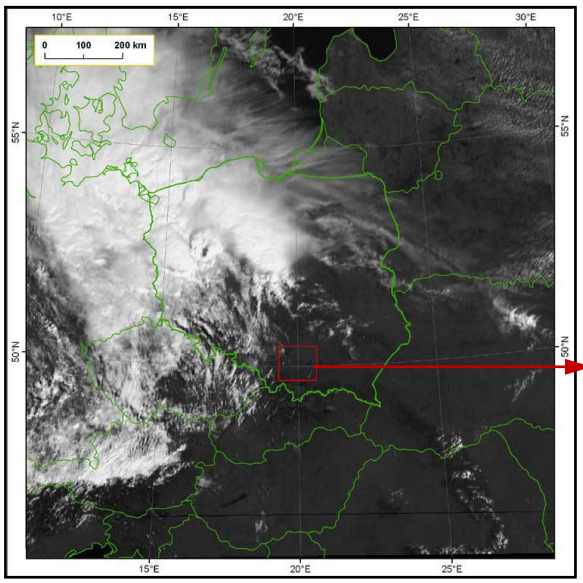

Fig. 1. 22.07.2007, 9:27 UTC, MSG2/SEVIRI HRV image, location of study area (red square)

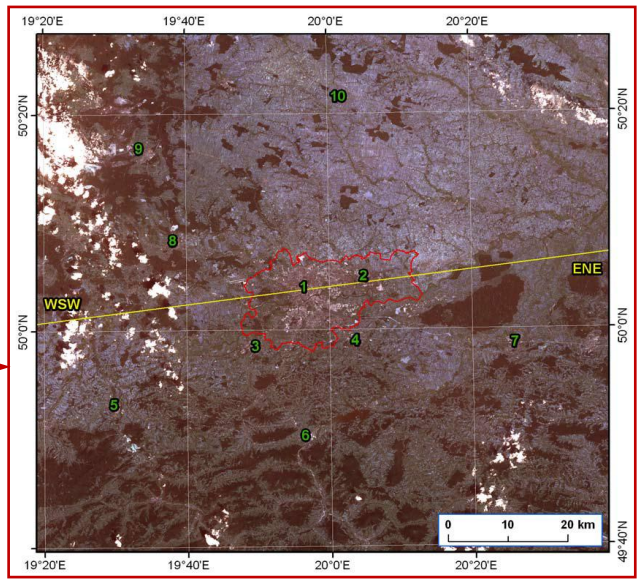

Fig. 2. Study area: Agglomeration of Krakow and its neighbourhood, Landsat-5 TM True colour composite [RGB = 321]

WEATHER CONDITIONS

Due to advection of very warm and humid air from the Mediterranean Region, July 22, 2007 was a hot day in Southern Poland (max. air temperature in Krakow 31.9 °C) coming after a warm night (min. air temperature 19.2 °C). There was a cold front, accompanied by heavy storms, approaching Krakow from the west (Fig 1). Between 9:00 and 10:00 UTC air temperature increased from 28.8°C to 31.9°C, relative humidity decreased from 61 % to 32 %, wind speed raised from 3 to 4 m/s and wind direction changed from ENE to SSW. Cloud cover was 1/8 and there were observed Stratocumulus stratiformis perlucidus at a height of 2 km (9:00 UTC) and Cumulus mediocris at a height of 0.8 km (10:00 UTC). The ground was dry.

COMPARATIVE ANALYSIS

Technical parameters of four operational satellites and sensors onboard them (Terra/MODIS, Meteosat-9/SEVIRI, NOAA-17/AVHRR, Landsat-5/TM) were stored in table 1. Thermal bands of considered sensors onboard environmental (Terra/MODIS and Landsat/TM) and weather (Meteosat/SEVIRI and NOAA/AVHRR) satellites as well as approximate spatial resolution of these bands over Krakow were compared to each other by drawing graphs (fig. 3 and fig. 4). Four LST maps were acquired (fig. 5 – 8) as a result of processing consisting of: geometric and radiometric correction, spectral radiance to radiant temperature conversion, radiant temperature to surface temperature recalculation (with atmospheric and emissivity correction). Land surface temperature was retrieved using selected LST algorithms (tab. 2). LST profile was drawn across the study area (fig. 2) to show temperature differences between each scene (fig. 9). Some advantages and disadvantages of different satellite sensors with respect to urban thermal conditions research were noticed (tab. 3).

Tab. 1. Technical details of satellite/sensor

Details	***Terra/MODIS***	***Meteosat-9 (MSG2)/SEVIRI***	***NOAA-17 /AVHRR***	***Landsat-5/TM***
Responsible organization	NASA	cooperation between ESA and EUMETSAT	cooperation between NOAA and NASA	joint effort of NASA and USGS

Launch date	December 18, 1999	December 21, 2005	June 24, 2002	March 1, 1984 - has significantly exceeded its designed life expectancy by over 22 years by 2009
Mission objective	environmental satellite with wide spectral resolution and viewing swaths, useful in a wide variety of Earth system science disciplines (including atmosphere sciences). It contributes to **Earth Observation System** (EOS)	established to ensure the continuity of meteorological observations from geostationary orbit, it contributes to **Global Meteorological Satellite Observing System**	in support to geostationary weather satellites, it provides nearly 1km resolution images a few times a day (especially meaningful for regions located in higher latitudes)	primarily designed to acquire images of land surface, most of all for change detection studies
Orbit parameters				
Altitude	705 km	approximately 35800 km	810 km	705 km
Type	polar orbiting, sun-synchronous	geostationary	near-polar, sun-synchronous	polar orbiting, sun-synchronous
Inclination	98.2°	0.0°	98.7°	98.2°
Orbital period	98.1 min.	–	101.2 min.	98.9 min.
Repeat cycle	**16 days** (equatorial crossing time 10:30 AM)	**15 min.** (5 min. – rapid scan mode)	data can be acquired **twice a day** in ascending and descending mode	**16 days** (equatorial crossing time 9:45 AM +/- 15 minutes)
Instrument parameters				
Sensor type	**MODIS** (MODerate resolution Imaging Spectroradiometer)	**SEVIRI** (Spinning Enhanced Visible and InfraRed Imager)	**AVHRR** (Advanced Very High Resolution Radiometer)	**TM** (Thematic Mapper)
Number of spectral bands	**36** (including 2 thermal bands: 31 and 32)	**12**: 1 visible broadband (HRV), 3 visible and near infrared, 2 water vapour and 6 infrared (including 2 thermal IR)	**6**: 3 visible and near-infrared, 3 infrared (including 2 thermal IR) Swath width: 3000 km	**7** (3 visible, 1 near-infrared, 2 mid-infrared and 1 thermal infrared)
*Swath width /*Field of view*	2330 km (cross track) by 10 km (along track at nadir)	*the whole hemisphere	3000 km	185 km
Spatial resolution	250x250 m (bands 1-2) 500x500 m (bands 3-7) **1000x1000 m** (bands 8-36)	at nadir: 1x1 km (HRV), **3x3 km** (other spectral bands)	**1.1x1.1 km**	30x30 m (**120x120 m** – thermal band)

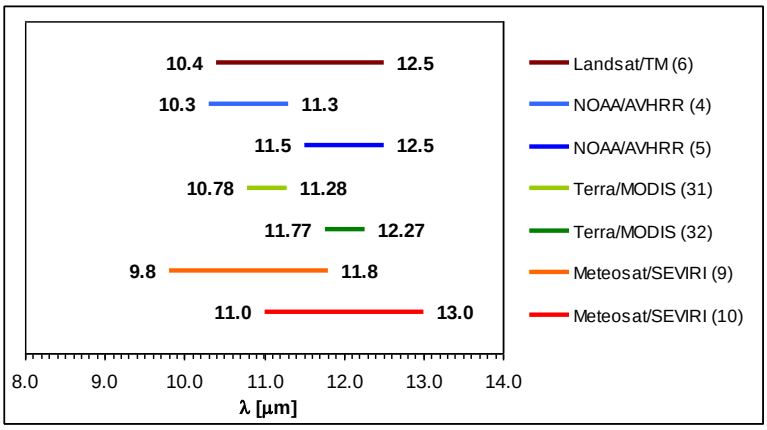

Fig. 3. Spectral ranges of thermal infrared bands

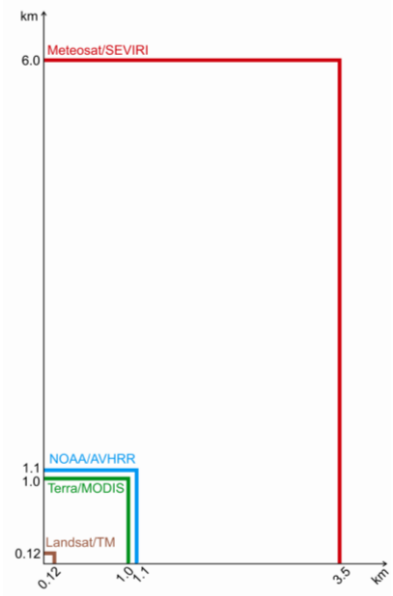

Fig. 4. Pixel sizes of thermal IR data

Tab. 2. Land surface temperature (LST) retrieval algorithms (Terra/MODIS, Meteosat-9 (MSG2)/SEVIRI, NOAA-17/AVHRR and Landsat-5/TM satellite data)

Satellite data	LST algorithms	Assumptions	References
Terra/MODIS	**$T_s = 0.5\,(T_{31} + T_{32})\,(A_1 + A_2\,(1 - \varepsilon) / \varepsilon + A_3\,\Delta\varepsilon / \varepsilon^2) + 0.5\,(T_{31} - T_{32})\,(B_1 + B_2\,(1 - \varepsilon) / \varepsilon + B_3\,\Delta e / \varepsilon^2) + C$** where : T_s – surface temperature calculated using split-window algorithm (channels: 31 & 32); T_{31}, T_{32} – radiant temperature obtained from 31 & 32 channels, respectively; ε – emissivity; A_1, A_2, A_3, B_1, B_2, B_3 – coefficients for LST algorithm; C – fractional vegetation cover coefficient.	**MOD11_L2** LST product used	Wan and Dozier 1996; Wan 1999
Meteosat-9 (MSG2)/SEVIRI	**$T_s = T_9 + a_1\,(T_9 - T_{10}) + a_2\,(T_9 - T_{10})^2 + a_3\,(1 - \varepsilon) + a_4\,W\,(1 - \varepsilon) + a_5\,\Delta\varepsilon + a_6\,W\,\Delta\varepsilon + a_6$** where : T_s – surface temperature calculated using split-window algorithm (channels: 9 & 10); T_9, T_{10} – radiant temperature obtained from 9 & 10 channels, respectively; ε – emissivity; W – total atmospheric water vapour content for standard mid-latitude summer atmosphere; a_1, a_2, a_3, a_4, a_5, a_6 – coefficients for LST algorithm.	**$\varepsilon = 0.9615$**; **$\Delta e = -0.007$**; **W = 2,92 g/cm^2;** **a_1, a_2, a_3, a_4, a_5, a_6 for 60° zenith observation angle**	Atitar et al. 2008
NOAA-17/ AVHRR	**$T_{45} = T_4 + 2.702\,(T_4 - T_5) - 0.582$** where : T_{45} – temperature calculated using split-window algorithm (channels: 4 & 5); T_4, T_5 – radiant temperature obtained from 4 & 5 channels, respectively.	**$\varepsilon = 0.97$**	Struzik 1998

Landsat-5/TM	$T_s = \gamma [\varepsilon^{-1} (\psi_1 L_{sensor} + \psi_2) + \psi_3] + \delta$ with $\gamma = \{c_2 L_{sensor} / T_{sensor}^2 + [\lambda^4 / c_1 L_{sensor} + \lambda^{-1}]\}^{-1}$ and $\delta = - \gamma L_{sensor} + T_{sensor}$ where : T_s – surface temperature calculated using generalized single-channel method; L_{sensor} – *at*-sensor radiance in W m^{-2} sr^{-1} μm^{-1}; T_{sensor} – at-sensor brightness temperature in K; γ – effective wavelength (11.457 μm for TM6 band); ε – emissivity; c_1, c_2 – constants (c_1 = 1.19104 10^8 W $\mu m^4 m^{-2}$ sr^{-1}; c_2 = 14387.7 μm K); ψ_1, ψ_1, ψ_1 – atmospheric functions obtained as a function of the total atmospheric water vapour content (W).	**ε = 0.97**; total atmospheric water vapour content for standard mid-latitude summer atmosphere **W = 2,92 g/cm^2**	Jiménez-Muñoz and Sobrino 2003

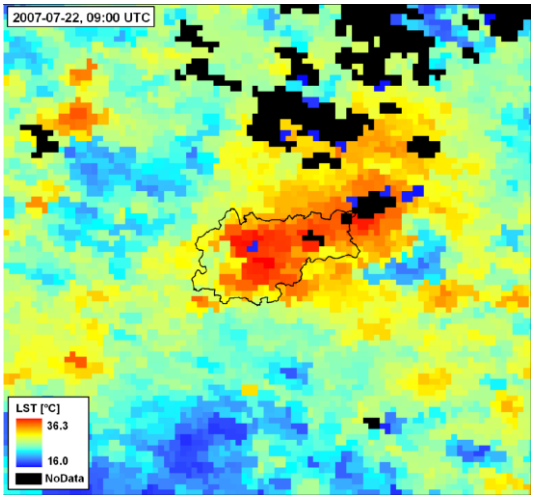

Fig. 5. Land surface temperature derived from Terra/MODIS data

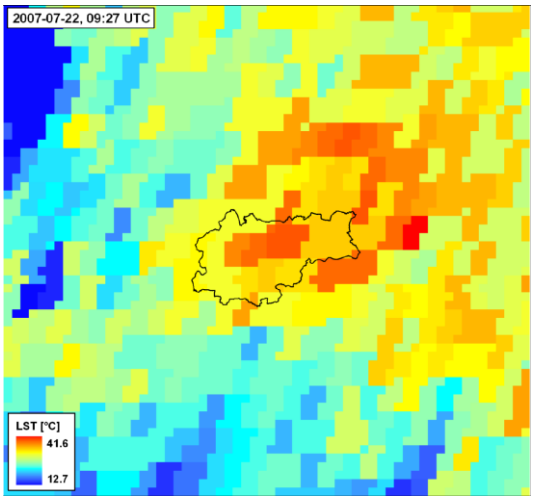

Fig. 6. Land surface temperature derived from Meteosat-9/SEVIRI data

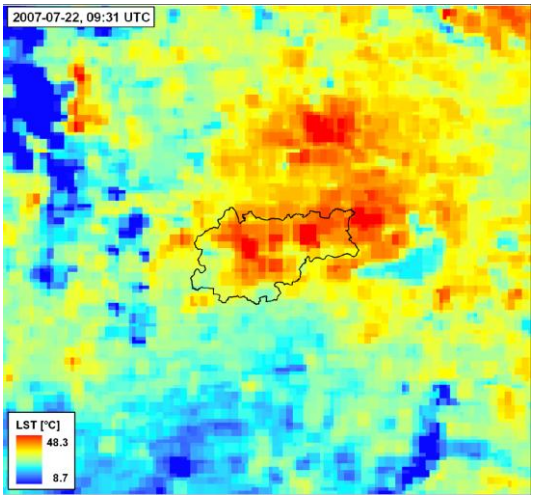

Fig. 7. Land surface temperature derived from NOAA-17/AVHRR data

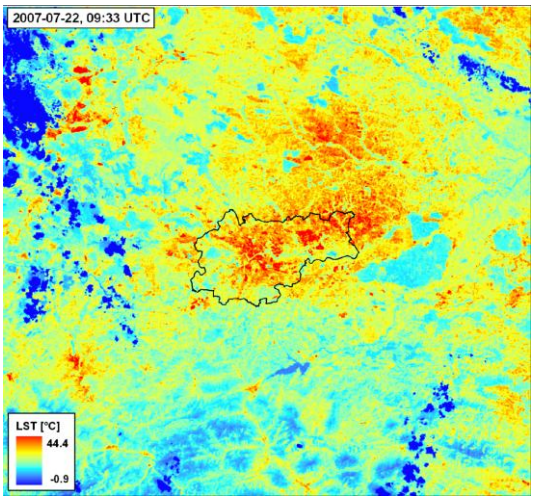

Fig. 8. Land surface temperature derived from Landsat-5/TM data

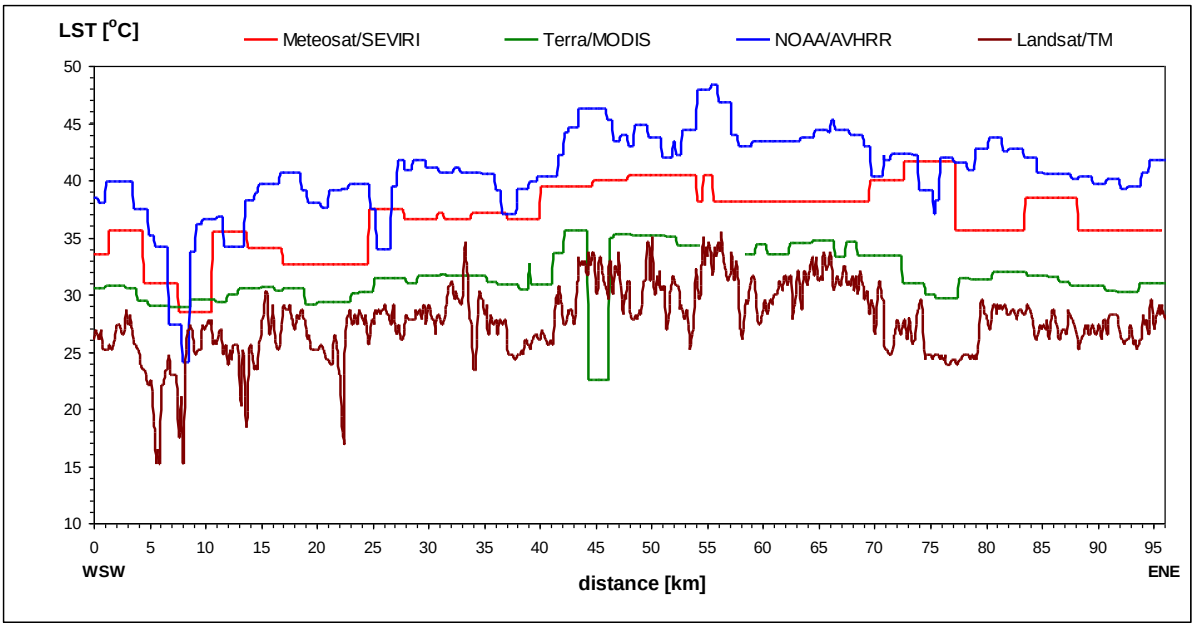

Fig. 9. Land surface temperature curves (LST profile)

Tab. 3. Advantages and disadvantages of satellite sensors (Terra/MODIS, Meteosat-9 (MSG2)/SEVIRI, NOAA-17/AVHRR and Landsat-5/TM) with respect to urban thermal conditions research

Satelite/Sensor	Advantages	Disadvantages
Terra/MODIS	+ A set of ready to use LST products available free of charge + Second MODIS sensor onboard Aqua satellite available + Another additional high resolution (90x90 m TIR) ASTER sensor installed onboard Terra satellite for comparative and/or more precise evaluation of land surface temperature distribution + Possible use of split-window algorithm (2 TIR channels: 31 and 32) to calculate LST + For MOD11_L2 product cloud cover masked out	– The prepared LST products may have some inaccuracies (e.g. for MOD11_L2 product [LST 5-Minute, 1 km Swath] used in the study some data gaps were identified in areas of high temperature emission) – Spatial resolution not good enough to see inner city land surface temperature pattern
Meteosat-9 (MSG2)/SEVIRI	+ Very high temporal resolution of data + Possible use of split-window algorithm (2 TIR channels: 10.8 and 12.0) to calculate LST + Gives possibility to compare UHI intensities of larger cities in the same time in continental scale + Land-SAF LST product (every 15 min.) available	– Much too low spatial resolution in order to detect UHI's of smaller cities – Not sufficient spatial resolution to assess UHI structure even in larger metropolis
NOAA-17/AVHRR	+ Spatial resolution sufficient to recognize some thermal contrasts within urban areas + Temporal resolution high enough to investigate diurnal and seasonal UHI changes + Possible use of split-window algorithm (2 TIR channels: 4 and 5) to calculate LST + AVHRR instrument installed also onboard NOAA-15, NOAA-16, NOAA-18, NOAA-19 and MetOp (more data available)	– Unstable spatial resolution because of radiometer scanning angle changes over study area – Irregular repeat cycle
Landsat-5/TM	+ Relatively high spatial resolution – more detailed land surface temperature pattern can be obtained + Made it possible to study relationship between land surface temperature and different land use types + Enables detection of single sources of the highest heat emission	– Very low temporal resolution (repeat cycle) – Only one and broad thermal infrared band (application of mono-window LST retrieval methods only)

CONCLUSIONS

This case study examines possible usage of land surface temperature (LST) retrievals from different satellite sensors in order to assess thermal conditions in urban-industrial area. It is rather unusual to acquire a set of cloud-free images at about the same time from all of the chosen satellite sensors. The comparison of four LST maps shows that thermal contrast within the considered study area (Krakow, Poland) is similar. However, there are significant differences between LST values estimated on the basis of Meteosat/SEVIRI, Terra/MODIS, NOAA/AVHRR and Landsat/TM data due to different algorithms. Despite the inequality of LST values derived from data obtained by different satellite sensors, the profile curves correspond with each other. They indicate higher LST values in the city centre and in the steelworks, and much lower LST values of forest and cloud tops.

It is very difficult to decide which of the applied algorithms is the most precise. To find an answer to this question satellite LST products should be validated by ground temperature measurements taken exactly in the time of image registration. Further test of available LST retrieval algorithms from Thermal IR data provided by different satellite sensor could make it possible to integrate all of the considered LST products in order to create one general map of spatial diversity of thermal conditions in agglomeration of Krakow.

Acknowledgements

ERDAS Imagine 9.3, ESRI ArcGIS Desktop 9.3 and VCS 2Met! used in this study for data processing, spatial analyses and visualization are licensed to the Institute of Meteorology and Water Management, Satellite Remote Sensing Centre. Additional software developed by Piotr Struzik (Head of the Satellite Remote Sensing Centre) was used to calculate land surface temperature from NOAA/AVHRR data. Authors would like to thank Piotr Struzik as well as all the other people who contributed to our research.

References

Terra/MODIS:

Mao K., Qin Z., Shi J., Gong P. (2005), A practical split-window algorithm for retrieving land-surface temperature from MODIS data. Int. J. Remote Sens. Vol. 26, No. 15, 3181-3204

MODIS Data Archive (MOD03 data download) - http://ladsweb.nascom.nasa.gov/data/search.html

MODIS Data Archive (MOD11_L2 data download) https://lpdaac.usgs.gov/lpdaac/products/modis_products_table/land_surface_temperature_emissivity/5_min_l2_swath_1km/mod11_l2

MODIS Level-1B Granule Images - http://modis-atmos.gsfc.nasa.gov/IMAGES/index.html

MODIS Rapid Response System - http://rapidfire.sci.gsfc.nasa.gov/realtime

Mito C. O., Laneve G., Castronuovo M. M., Ulivieri C. (2006), Derivation of land surface temperatures from MODIS data using the general split-window technique. Int. J. Remote Sens. Vol. 27, No. 12, 2541-2552

Terra Orbit Tracks - http://www.ssec.wisc.edu/datacenter/terra

Trigo, I. F., Monteiro I. T., Olesen F., Kabsch E. (2008), An assessment of remotely sensed land surface temperature. J. Geophys. Res., 113, D17108, doi:10.1029/2008JD010035

Wan Z. (1999), MODIS Land-Surface Temperature Algorithm Theoretical Basis Document (LST ATBD) Version 3.3. Institute ICESS, University of California, Santa Barbara (http://www.icess.ucsb.edu/modis/atbd-mod-11.pdf)

Wan Z. (2009), Collection-4 MODIS Land Surface Temperature Products Users' Guide. ICESS, University of California, Santa Barbara (http://www.icess.ucsb.edu/modis/LstUsrGuide/usrguide.html)

Wan Z. (2009), Collection-5 MODIS Land Surface Temperature Products Users' Guide. ICESS, University of California, Santa Barbara (http://www.icess.ucsb.edu/modis/LstUsrGuide/usrguide.html)

Wan Z., Dozier J. (1996), A generalized split-window algorithm for retrieving land-surface temperature from space. IEEE Transactions on Geoscience and Remote Sensing, 34, pp. 892–905

Wang K., Wan Z., Wang P., Sparrow M., Liu J., Haginoya S. (2007), Evaluation and improvement of the MODIS land surface temperature/emissivity products using ground-based measurements at a semi-desert site on the western Tibetan Plateau. Int. J. Remote Sens. Vol. 28, No. 11, 2549-2565

Meteosat (MSG)/SEVIRI:

Atitar M., Sobrino J.A., Soria G., Wigneron J.P., Jiménez-Muñoz J.C., Julien Y., Belen Ruescas A. (2008), Land surface temperature retrieved from SEVIRI/MSG2 data: algoritm and validation. Proc. 2008 EUMETSAT Meteorological Satellite Conference, Darmstadt, Germany 8-12 Sept. 2008

Dash P., Giittsche F. M., Olesen F. S. (2003), Emissivity and temperature estimation from MSG SEVIRI data; data method validation with simulated and NOAA 14 AVHRR data. Adv. Space Res. Vol. 32, No. 11, 2241-2246

Peres L. F., DaCamara C. C. (2004), Land surface temperature and emissivity estimation based on the two temperature method: sensitivity analysis using simulated MSG/SEVIRI data. Remote Sens. Environ. 91, 377-389

Product User Manual PUM LST Land Surface Temperature. LSA SAF, Ref. SAF/LAND/IM/ PUM_LST/2.2, Issue: Version 2.2, Date: 15 July 2008 (http://landsaf.meteo.pt/algorithms.jsp?seltab=0&starttab=0)

Sobrino J. A., Romaguera M. (2004), Land surface temperature retrieval from MSG1-SEVIRI data. Remote Sens. Environ. 92, 247-254

Sun D., Pinker R. T. (2007), Retrieval of surface temperature from the MSG-SEVIRI observations: Part I. Methodology. Int. J. Remote Sens. Vol. 28, No. 23, 5255-5272

NOAA/AVHRR:

Chrysoulakis N., Cartalis C. (2002), Improving the estimation of land surface temperature for the region of Greece: adjustment of a split window algorithm to account for the distribution of precipitable water. Int. J. Remote Sens. Vol. 23, No. 5, 871-880

Gallo K. P., McNab A. L, Karl T. R., Brown J. F., Hood J. J., Tarpley J. D. (1993), The use of NOAA AVHRR data for assessment of the urban heat island effect, J. Appl. Meteor., 32, 899-908

Kerényi J., Putsay M.(2000), Investigation of land surface temperature algorithms using NOAA AVHRR images. Adv. Space Res. Vol. 26, No. 7, 1077-1080

NOAA KLM User's Guide - http://www.ncdc.noaa.gov/oa/pod-guide/ncdc/docs/klm/index.htm

Streutker D. R. (2002), A remote sensing study of the urban heat island of Houston, Texas, Int. J. Remote Sens., 23, 2595-2608

Struzik P. (1998), Application of the AVHRR/NOAA satellite information for urban heat island investigation. Acta Univ. Lodz., Folia Geogr. Phys. 3, 161-171 (article in Polish, summary in English)

Landsat/TM:

Barsi J. A., Hook S. J., Schott J. R., Raqueno N. G., Markham B. L. (2007), Landsat-5 Thematic Mapper Thermal Band Calibration Update. IEEE Geoscience and Remote Sensing Letters, vol. 4, no. 4, 552 – 555

Chander G., Markham B.L., Barsi J.A. (2007), Revised Landsat-5 Thematic Mapper Radiometric Calibration. IEEE Geoscience and Remote Sensing Letters, vol. 4, no. 3, 490-494

Chander G., Markham B.L., Helder D.L., (2009), Summary of current radiometric calibration coefficients for Landsat MSS, TM, ETM+, and EO-1 ALI sensors. Remote Sensing of Environment, vol. 113, no. 5, 893–903

Jiménez-Muñoz J. C., Sobrino J. A. (2003), A generalized single-channel method for retrieving land surface temperature from remote sensing data, J. Geophys. Res., 108 (D22), 4688, doi:10.1029/2003JD003480

Landsat data archive 1 - http://glovis.usgs.gov

Landsat data archive 2 - http://earthexplorer.usgs.gov

Landsat Program homepage - http://landsat.gsfc.nasa.gov

Landsat Missions webpage - http://landsat.usgs.gov

Landsat 7 Science Data User's Handbook - http://landsathandbook.gsfc.nasa.gov/handbook/handbook_toc.html

Sobrino J. A., Jiménez-Muñoz J. C., Paolini L. (2004), Land surface temperature retrieval from LANDSAT TM 5. Remote Sens. Environ. 90, 434-440

Weng Q., Lu D., Schubring J. (2004), Estimation of land surface temperature–vegetation abundance relationship for urban heat island studies. Remote Sens. Environ. 89, 467-483